Structural, Electrochemical, and Spectroscopic Characterization of a Redox Pair of Sulfite-Based Polyoxotungstates: α-[W 18 O 54 (SO 3) 2] 4 - and α-[W 18 O 54 (SO 3) 2] 5 -

ARTICLE *in* INORGANIC CHEMISTRY · APRIL 2007

Impact Factor: 4.76 · DOI: 10.1021/ic062067e · Source: PubMed

Inorg. Chem. **2007**, *46*, 3502–3510

Structural, Electrochemical, and Spectroscopic Characterization of a Redox Pair of Sulfite-Based Polyoxotungstates: α-$[W_{18}O_{54}(SO_3)_2]^{4-}$ and α-$[W_{18}O_{54}(SO_3)_2]^{5-}$

Nigel Fay,[†] Alan M. Bond,*[,†] Carole Baffert,[†] John F. Boas,[‡] John R. Pilbrow,[‡] De-Liang Long,[§] and Leroy Cronin*[,§]

School of Chemistry, Monash University, Clayton, Victoria 3800, Australia, School of Physics, Monash University, Clayton, Victoria 3800, Australia, and WestCHEM, Department of Chemistry, The University of Glasgow, Glasgow, G128QQ, U.K.

Received October 29, 2006

The synthesis, isolation, and structural characterization of the fully oxidized sulfite-based polyoxotungstate cluster $(Pr_4N)_4\{\alpha$-$[W_{18}O_{54}(SO_3)_2]\}\cdot 2CH_3CN$ and the one-electron reduced form $(Pr_4N)_5\{\alpha$-$[W_{18}O_{54}(SO_3)_2]\}\cdot 2CH_3CN$ has been achieved. α-$[W_{18}O_{54}(SO_3)_2]^{5-}$ was obtained as a Pr_4N^+ salt by reducing the "Trojan Horse" $[W_{18}O_{56}(SO_3)_2(H_2O)_2]^{8-}$ cluster via a template orientation transformation. Acetonitrile solutions of pure α-$[W_{18}O_{54}(SO_3)_2]^{5-}$ also were prepared electrochemically by one-electron bulk reductive electrolysis of α-$[W_{18}O_{54}(SO_3)_2]^{4-}$. Cyclic voltammetry of α-$[W_{18}O_{54}(SO_3)_2]^{4-}$ and α-$[W_{18}O_{54}(SO_3)_2]^{5-}$ in CH_3CN (0.1 M Hx_4NClO_4) produces evidence for an extensive series of reversible one-electron redox processes, that are associated with the tungsten–oxo framework of the polyoxometalate cluster. Hydrodynamic voltammograms in CH_3CN exhibit the expected sign and magnitude of the steady-state limiting current values for the α-$[W_{18}O_{54}(SO_3)_2]^{4-/5-/6-}$ series and confirm the existence of a stable one-electron reduced species, α-$[W_{18}O_{54}(SO_3)_2]^{5-}$. Employment of the Randles–Sevcik (cyclic voltammetry) and Levich (rotating disk electrode) equations at a glassy carbon electrode ($d = 3$ mm) enable diffusion coefficient values of 3.7 and 3.8 $\times 10^{-6}$ cm^2 s^{-1} to be obtained for α-$[W_{18}O_{54}(SO_3)_2]^{4-}$ and α-$[W_{18}O_{54}(SO_3)_2]^{5-}$, respectively. The tungsten polyoxometalates are highly photoactive, since measurable photocurrents and color changes are detected for both species upon irradiation with white light. EPR spectra obtained from both acetonitrile solution and solid samples, down to temperatures as low as 2.3 K, of the chemically and electrochemically prepared one-electron reduced species provided evidence that the unpaired electron in α-$[W_{18}O_{54}(SO_3)_2]^{5-}$ is delocalized over a number of atoms in the polyoxometalate structure, even at very low temperatures.

Introduction

Since their discovery in the 19th century by Berzelius,[1] polyoxometalates have been extensively studied. Their wide-ranging structural, redox, and photochemical characteristics, high ionic charge, conductivity, and molecular weights are the primary reasons they are utilized in fields such as medicinal chemistry,[2–4] surface and solid-state chemistry,[5] materials science,[6–8] sensor technology, and catalysis.[9–12] Dawson or Wells−Dawson polyoxometalates, of general formula $[M_{18}O_{54}(XO_4)_2]^{m-}$ (where M = Mo, W and X = P, S), were first discovered in 1953 by Dawson,[13] having been previously postulated by Wells.[14] The Dawson-type poly-

* To whom correspondence should be addressed. E-mail: alan.bond@sci.monash.edu.au (A.M.B.); L.Cronin@chem.gla.ac.uk (L.C.).
† School of Chemistry, Monash University.
‡ School of Physics, Monash University.
§ The University of Glasgow.

(1) Pope, M. T. *Heteropoly and Isopoly Oxometalates*; Springer: New York, 1983.
(2) Rhule, J. T.; Hill, C. L.; Judd, D. A. *Chem. Rev.* **1998**, *98*, 327.
(3) Aguey-Zinsou, K. F.; Bernhardt, P. V.; Kappler, U.; McEwan, A. G. *J. Am. Chem. Soc.* **2003**, *125*, 530.
(4) Hasenkopf, B. *Front. Biosci.* **2005**, *10*, 275.
(5) Klemperer, W. G.; Wall, C. G. *Chem. Rev.* **1998**, *98*, 297.
(6) Ogliaro, F.; De Visser, S. P.; Cohen, S.; Sharma, P. K.; Shaik, S. *J. Am. Chem. Soc.* **2002**, *124*, 2806.
(7) Yamase, T. *Chem. Rev.* **1998**, *98*, 307.
(8) Pope, M. T.; Mueller, A. *Angew. Chem., Int. Ed.* **1991**, *103*, 56.
(9) Mizuno, N.; Misono, M. *Chem. Rev.* **1998**, *98*, 199.
(10) Hill, C. L. *Angew. Chem., Int. Ed.* **2004**, *43*, 402.
(11) Hill, C. L. *Comprehensive Coord. Chem. II* **2004**, *4*, 679.
(12) Sadakane, M.; Steckhan, E. *Chem. Rev.* **1998**, *98*, 219.
(13) Dawson, B. *Acta. Crystallogr.* **1953**, *6*, 113.
(14) Wells, A. F. *Structural Inorg. Chem.*; Oxford University Press; Oxford, 1945; p 344.

10.1021/ic062067e CCC: $37.00
Published on Web 03/29/2007

oxometalate is very closely related to the Keggin-type.[1] From the M_{12} structure of the Keggin, three MO_6 octahedra are removed, resulting in a M_9 unit. This M_9 unit is one-half of the M_{18} Dawson structure, and upon linkage via corner sharing with a similar unit the α-$[M_{18}O_{54}(XO_4)_2]^{m-}$ Dawson is formed. The D_{3h} symmetry of the α-isomer can be changed to the D_{3d} symmetry of the β-isomer by rotation of one-half of the structure by 60°. As with the Keggin-type polyoxometalates, further isomers are possible by successive rotations of the M_3O_{13} units which are present at the end of each of the α- and β-isomers.[1]

To date, a large number of papers have been published that describe the synthesis and characterization of conventional Dawson polyoxometalates, whereby two tetrahedral anions are incorporated into the structure, for example PO_4^{3-},[15] SO_4^{2-},[16−19] and ClO_4^-.[20,21] However, relatively few cases have been reported in which a non-tetrahedral anion, such as the pyramidal sulfite anion, SO_3^{2-}, is a part of the caged Dawson structure. Previously known Dawson-like clusters containing examples of pyramidal anions include BiO_3^{3-} [22] and AsO_3^{3-} [27] and the di-tetrahedral anion $P_2O_7^{4-}$.[23−26] Members of our group recently synthesized and reported on the crystallography of the α- and β-polyoxomolybdosulfites[28] and exploited the fact that the SO_3^{2-} anion is quite a polarizable soft Lewis base. Differences in the relative orientations of the two SO_3^{2-} anions, in the α- and β-isomers, and their adjoined M_9 units has been described, along with the dimensions of the S−S distances within the caged structure, as have the electrochemical and electronic properties.[29] The synthesis and isolation of the α-form of the sulfite-based polyoxotungstate $[W_{18}O_{54}(SO_3)_2]^{4-}$ cluster, using the tetrabutylammonium cation as the crystallization cation was reported.[30] When K^+ was employed as the cation to isolate this cluster, a new structural form of sulfite polyoxometalate, $[W_{18}O_{56}(SO_3)_2(H_2O)_2]^{8-}$, the so-called "Trojan Horse" was obtained.[30] The difference between $[W_{18}O_{54}(SO_3)_2]^{4-}$ and $[W_{18}O_{56}(SO_3)_2(H_2O)_2]^{8-}$ lies in the orientation of the two sulfite templates inside the clusters and therefore the numbers of terminal ligands on the tungsten centers.

The synthesis, structural, and electrochemical characterization of the sulfate polyoxometalate $[W_{18}O_{54}(SO_4)_2]^{4-}$ has been reported.[16,17,31−32] In the case of this sulfate system, upon controlled potential electrolysis of either the α- or γ^*-$[W_{18}O_{54}(SO_4)_2]^{4-}$ isomer, the one-electron reduced species, α-$[W_{18}O_{54}(SO_4)_2]^{5-}$, rather than the γ^*-isomer is formed.[31] In the present study, the synthesis, structural, and electrochemical characterization of a redox couple in the α-form of the fully oxidized sulfite polyoxometalate, $(Pr_4N)_4\{\alpha$-$[W_{18}O_{54}(SO_3)_2]\}\cdot 2CH_3CN$, and the one-electron reduced species $(Pr_4N)_5\{\alpha$-$[W_{18}O_{54}(SO_3)_2]\}\cdot 2CH_3CN$ (Pr_4N^+ = tetrapropylammonium), are described. The electronic properties of the cluster are elucidated by EPR spectroscopy in order to address the delocalization of the unpaired electron of the tungsten−oxo framework. As well as exhibiting an extensive series of one-electron reduction steps, as ascertained by voltammetric measurements, a high level of photoactivity is also established by irradiating samples with visible light, which may lead to their application in solar energy devices.[33] This paper therefore reports the first detailed investigation of the redox chemistry and spectroscopy of novel tungsten sulfite polyoxotungstates, and data obtained are compared to that established for the previously reported molybdenum sulfite analogue[29] and related sulfate species.[16]

Experimental Section

Synthesis. Crystalline samples of the one-electron reduced form of the tungstosulfite polyoxometalate $(Pr_4N)_5\{\alpha$-$[W_{18}O_{54}(SO_3)_2]\}\cdot 2CH_3CN$ were produced as follows. A few drops of HCl (4 M) were added to a solution of $K_7Na[W_{18}O_{56}(SO_3)_2(H_2O)_2]\cdot 20H_2O$ (0.8 g, 0.16 mmol) in H_2O (50 mL) to bring the pH to 1, and this was followed by the addition of $Na_2S_2O_4$ (0.1 g). The resulting mixture was stirred for 5 min, and a solution of Pr_4NBr (1.2 g) in water (10 mL) was added. The blue precipitate was collected by centrifuging, washed with water and ethanol, and dried under vacuum. Recrystallization of the blue product in acetonitrile afforded blue needle crystals of $(Pr_4N)_5\{\alpha$-$[W_{18}O_{54}(SO_3)_2]\}\cdot 2CH_3CN$. Yield 0.58 g (69%). A few colorless crystals of a byproduct were identified as $(Pr_4N)_4\{\alpha$-$[W_{18}O_{54}(SO_3)_2]\}\cdot 2CH_3CN$ which also can be obtained quantitively by the process described above but without using the reducing agent $Na_2S_2O_4$. For $(Pr_4N)_5\{\alpha$-$[W_{18}O_{54}(SO_3)_2]\}\cdot 2CH_3CN$ IR (KBr disk): ν/cm^{-1}: 3432, 2969, 2877, 1629, 1484, 1383, 988, 917, 789; anal. calcd for $C_{62}H_{143}N_6O_{60}S_2W_{18}$ (losing one CH_3CN): C 14.03, H 2.72, N 1.58; found: C 13.88, H 2.66, N 1.58%. For $(Pr_4N)_4\{\alpha$-$[W_{18}O_{54}(SO_3)_2]\}$ IR (KBr disk): ν/cm^{-1}: 3429, 2965, 2874, 1483, 1384, 988, 918, 798; anal. calcd for $C_{50}H_{115}N_5O_{60}S_2W_{18}$ (losing one CH_3CN): C 11.73, H 2.26, N 1.37; found: C 11.57, H 2.17, N 1.22%.

X-ray Crystallographic Studies. Suitable single crystals of $(Pr_4N)_5\{\alpha$-$[W_{18}O_{54}(SO_3)_2]\}\cdot 2CH_3CN$ and $(Pr_4N)_4\{\alpha$-$[W_{18}O_{54}(SO_3)_2]\}\cdot 2CH_3CN$ were selected from the crystallization and were mounted on a thin glass fiber using Fomblin oil. X-ray intensity data were measured on a Bruker ApexII-CCD diffractometer [λ-(W K_α) = 0.71073 Å]. Data were processed using SAINT software. Structure solution and refinement were carried out with SHELXS-

(15) Holscher, M.; Englert, U.; Zibrowius, B.; Holderich, W. *Angew. Chem., Int. Ed.* **1994**, *106*, 2552.
(16) Zhang, J.; Bond, A. M.; Richardt, P. J. S.; Wedd, A. G. *Inorg. Chem.* **2004**, *43*, 8263.
(17) Richardt, P. J. S.; Gable, R. W.; Bond, A. M.; Wedd, A. G. *Inorg. Chem.* **2001**, *40*, 703.
(18) Way, D. M.; Cooper, J. B.; Sadek, M.; Vu, T.; Mahon, P. J.; Bond, A. M.; Brownlee, R. T. C.; Wedd, A. G. *Inorg. Chem.* **1997**, *36*, 4227.
(19) Neier, R.; Trojanowski, C.; Mattes, R. *J. Chem. Soc., Dalton Trans.* **1995**, 2521.
(20) Herbstein, F. H.; Marsh, R. E. *Acta Crystallogr.* **1998**, *B54*, 677.
(21) Zhu, S.; Yue, B.; Shi, X.; Gu, Y.; Liu, J.; Chen, M.; Huang, Y. *J. Chem. Soc., Dalton Trans.* **1993**, 3633.
(22) Ozawa, Y.; Sasaki, Y. *Chem. Lett.* **1987**, 923.
(23) Hori, T.; Sugiyama, M.; Himeno, S. *Chem. Lett.* **1988**, 1017.
(24) Himeno, S.; Saito, A.; Hori, T. *Inorg. Chem.* **1990**, *63*, 1602.
(25) Kortz, U.; Pope, M. T. *Inorg. Chem.* **1994**, *33*, 5643.
(26) Kortz, U. *Inorg. Chem.* **2000**, *39*, 623.
(27) Jeannin, Y.; Martin-Frere, J. *Inorg. Chem.* **1979**, *18*, 3010.
(28) Long, D. L.; Kogerler, P.; Cronin, L. *Angew. Chem., Int. Ed.* **2004**, *43*, 1817.
(29) Baffert, C.; Boas, J. F.; Bond, A. M.; Kogerler, P.; Long, D. L.; Pilbrow, J. R.; Cronin, L. *Eur. Chem. J.* **2006**, *12*, 8472.
(30) Long, D. L.; Abbas, H.; Kogerler, P.; Cronin, L. *Angew. Chem., Int. Ed.* **2005**, *44*, 3415.
(31) Richardt, P. J. S.; White, J. M.; Tregloan, P. A.; Bond, A. M.; Wedd, A. G. *Can. J. Chem.* **2001**, *79*, 613.
(32) Himeno, S.; Tatewaki, H.; Hashimoto, M. *Bull. Chem. Soc. Jpn.* **2001**, *74*, 1623.
(33) Green, M. A. *Energy Policy* **2000**, 28.

Table 1. Crystallographic Data for $(Pr_4N)_5\{\alpha\text{-}[W_{18}O_{54}(SO_3)_2]\}\cdot 2CH_3CN$ and $(Pr_4N)_4\{\alpha\text{-}[W_{18}O_{54}(SO_3)_2]\}\cdot 2CH_3CN$

	α-$[W_{18}O_{54}(SO_3)_2]^{5-}$	α-$[W_{18}O_{54}(SO_3)_2]^{4-}$
empirical formula	$C_{64}H_{146}N_7O_{60}S_2W_{18}$	$C_{52}H_{118}N_6O_{60}S_2W_{18}$
M (g/mol)	5347.3	5160.94
cryst syst	monoclinic	monoclinic
a (Å)	16.4863(12)	25.2744(9)
b (Å)	22.0781(15)	18.0781(7)
c (Å)	33.587(2)	25.9777(9)
β (deg)	98.137(4)	109.794(2)
space group	$P2_1/n$	$P2_1/n$
V (Å^3)	12102.0(15)	11168.3(7)
Z	4	4
ρ_{calcd} (g/cm^3)	2.935	3.069
μ (cm^{-1})	17.147	18.574
T (K)	100(2)	180(2)
data/params	12 643/1086	20 223/1262
R1; wR2[a]	0.0716; 0.1594	0.0479; 0.1067

[a] $R1 = \sum||F_o| - |F_c||/\sum|F_o|$. $wR2 = \{\sum[w(F_o^2 - F_c^2)^2]/\sum[w(F_o^2)^2]\}^{1/2}$.

97 and SHELXL-97 via WinGX. Empirical absorption corrections for incident and diffracted beam absorption effects were applied. The structure was solved by a combination of direct methods and difference Fourier syntheses and refined against F^2 by the full-matrix least-squares technique. The W and S atoms were initially located by direct methods, and all other non-H atoms were found by successive difference Fourier syntheses. Most non-H atoms were refined anisotropically. In $(Pr_4N)_5\{\alpha\text{-}[W_{18}O_{54}(SO_3)_2]\}\cdot 2CH_3CN$, due to high thermal disorder in the Pr_4N^+ cation positions, these were only approximately refined utilizing suitable restraints of the N−C and C−C distances. However, although the crystallographic analysis does result in relatively high R values as a result of these disorders, the cluster is well defined without any disorder on W, S, and O positions. In $(Pr_4N)_4\{\alpha\text{-}[W_{18}O_{54}(SO_3)_2]\}\cdot 2CH_3CN$, both cluster and cations are well defined without disorder. Only disorder models were applied to solvent molecules. Crystal data, data collection parameters, and refinement statistics for α-$[W_{18}O_{54}(SO_3)_2]^{4-}$ and α-$[W_{18}O_{54}(SO_3)_2]^{5-}$ are listed in Table 1. The CCDC reference numbers for α-$[W_{18}O_{54}(SO_3)_2]^{4-}$ and α-$[W_{18}O_{54}(SO_3)_2]^{5-}$ are 641152 and 641151, respectively.

Electrochemistry. Acetonitrile (CH_3CN; Merck; Analytical Grade) and tetrahexylammonium perchlorate (Hx_4NClO_4; Fluka; Puriss Grade) were used as the solvent and electrolyte, respectively. Triflic acid (CF_3COOH; 3 M; Anhydrous) was employed as a proton source. A BAS Epsilon CS3 Electrochemical Workstation was employed for all voltammetric experiments. These experiments were performed at 20 (±2) °C, in a single-compartment three-electrode cell. A silver wire quasi-reference electrode, referenced against the IUPAC-recommended ferrocene (Fc/Fc^+) internal reference, was used to report potentials against a glassy carbon disk (d = 3 mm) working electrode. Potentials are reported versus Fc/Fc^+ with a precision of ±5 mV. Data obtained at platinum and gold working electrodes are not reported but displayed almost identical voltammetric behavior. The glassy carbon working electrode was polished successively with 1.0, 0.3, and 0.05 μm aqueous alumina slurries and sonicated in distilled water and rinsed with acetone after each polishing step. For rotating-disc electrode experiments, a variable-speed rotator was employed (BAS RDE-2). The auxiliary electrode material was a 1 mm diameter platinum wire. All solutions were degassed with high-purity argon for 15 min prior to electrochemical experiments.

Bulk electrolysis was employed in the electrochemical preparation of the one-electron reduced species, α-$[W_{18}O_{54}(SO_3)_2]^{5-}$. In this case, the working electrode was a BAS glassy carbon gauze basket, which was placed in a glass cylinder with a porous frit in the base. This cylinder was then placed symmetrically inside a platinum gauze basket, which was used as the auxiliary electrode. The reference electrode employed was the same as used for cyclic voltammetry. The working electrode compartment was filled with α-$[W_{18}O_{54}(SO_3)_2]^{4-}$ dissolved in CH_3CN (0.1 M Hx_4NClO_4, where Hx_4N^+ is tetrahexylammonium), while the auxiliary electrode compartment was filled with CH_3CN (0.1 M Hx_4NClO_4). During the course of the bulk electrolysis experiments, the working electrode was held at the appropriate potential to generate the reduced species, while the solution was stirred vigorously. The electrolysis was stopped when the current achieved a value of 1% of the initial current. The polyoxometalate underwent a green to blue color change upon reduction, typical of these species.[1]

Electron Paramagnetic Resonance Spectroscopy. EPR experiments were carried out with a Bruker ESP 380E FT/CW X-band EPR spectrometer using either a standard rectangular TE_{012} cavity or a Bruker ER 4118 high Q cylindrical resonator. Measurements at 77 K employed a Bruker liquid nitrogen finger dewar inserted in the rectangular cavity. For temperatures between 106 and 295 K, a nitrogen gas flow insert dewar was used. At least 5 min was allowed for thermal equilibrium to be established. Temperatures between 2.3 and ~100 K were achieved with the cylindrical resonator inserted in an Oxford instruments CF 935 cryostat. Temperatures in this range were calibrated against a germanium thermometer using a carbon resistor as transfer standard. Microwave frequencies were measured with an EIP Microwave 548A frequency counter and g-values were determined with reference to the F^+ line in CaO (g = 2.0001 ± 0.0002).[34] EPR spectral simulations were performed using the SOPHE software suite.[35]

Photochemistry. In photoelectrochemical experiments, light was introduced from below the electrochemical cell.[36] In the case of the photocurrents of α-$[W_{18}O_{54}(SO_3)_2]^{4-}$, the potential was held at +400 mV (vs Fc/Fc^+), a value at which the α-$[W_{18}O_{54}(SO_3)_2]^{4-}$ anion is not electroactive, in the absence of light. Currents were recorded at the applied potential prior to and after irradiation in order to monitor changes in redox level of bulk solutions of the polyoxometalate on exposure to light. The distance between the working electrode surface and the light source was 1.5 cm. The solution layer thickness between the working electrode and the bottom of the cell was 0.5 cm. For these experiments, the solution contained the polyanion salts (0.2 mM) dissolved in dimethylformamide (DMF; Fluka; Puriss Grade), with 0.1 M Bu_4NPF_6 as the electrolyte. The solution was stationary throughout the course of photoelectrochemical experiments. Irradiation of samples with white light (312−700 nm) was achieved with a Polilight PL6 source (Rofin).[37] The total power output of the lamp at the end of the liquid light guide was 7 W.

Results and Discussion

Syntheses. Dissolution of the $[W_{18}O_{56}(SO_3)_2(H_2O)_2]^{8-}$ 'Trojan Horse' cluster in water and reduction with $Na_2S_2O_4$ and addition of Pr_4NBr led to the reduced α-form $(Pr_4N)_5$-

(34) Wertz, J. E., Orton, J. W., Auzins, P. *Discuss. Faraday Soc.* **1961**, *31*, 140.
(35) Hanson, G. R.; Gates, K. E.; Noble, C. J.; Griffin, M.; Mitchell, A.; Benson, S. *J. Inorg. Biochem.* **2004**, *98*, 903.
(36) Fay, N.; Hultgren, V. M.; Wedd, A. G.; Keyes, T. E.; Leane, D. L.; Bond, A. M. *Dalton Trans.* **2006**, 4218.
(37) Rofin Polilight PL6 manual. www.rofin.com.au
(38) Zhang, J.; Bond, A. M.; MacFarlane, D. R.; Forsyth, S. A.; Pringle, J. M.; Mariotti, A. W. A.; Glowinski, A. F.; Wedd, A. G. *Inorg. Chem.* **2005**, *44*, 5123.

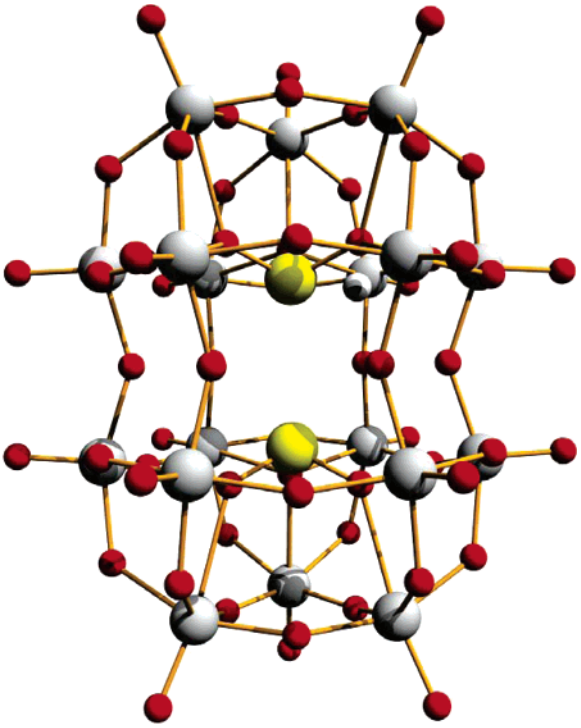

Figure 1. Structure of α-$[W_{18}O_{54}(SO_3)_2]^{4-}$ as determined by X-ray crystallography; the α-$[W_{18}O_{54}(SO_3)_2]^{5-}$ cage is isostructural.

$\{\alpha\text{-}[W_{18}O_{54}(SO_3)_2]\}\cdot 2CH_3CN$ being obtained, which has the same framework geometry as that of α-$[W_{18}O_{54}(SO_3)_2]^{4-}$ in $(Bu_4N)_4[W_{18}O_{54}(SO_3)_2]$ previously reported.[30]

$$[W_{18}O_{56}(SO_3)_2(H_2O)_2]^{8-} + e^- + 4\,H^+ \xrightarrow{Na_2S_2O_4} [W_{17}{}^{VI}W^{V}O_{54}(SO_3)_2]^{5-} + 2H_2O$$

During the synthesis of α-$[W_{18}O_{54}(SO_3)_2]^{5-}$ (see Experimental Section), α-$[W_{18}O_{54}(SO_3)_2]^{4-}$ was also obtained as the Pr_4N^+ salt as a byproduct. This fully oxidized material has the same non-reduced cluster α-$[W_{18}O_{54}(SO_3)_2]^{4-}$ framework as the $(Bu_4N)_4[\alpha\text{-}W_{18}O_{54}(SO_3)_2]$ salt described previously.[30] Therefore, it is interesting to note that the present synthetic process verified that the sulfite templates can change their orientation to suit different cations and the mixed-valence reduced state of the cluster shell.

Structural Analysis. $(Pr_4N)_5\{\alpha\text{-}[W_{18}O_{54}(SO_3)_2]\}\cdot 2CH_3CN$ crystallizes as a monoclinic system with one α-$[W_{18}O_{54}(SO_3)_2]^{5-}$ anion and five Pr_4N^+ cations found in the asymmetric unit plus some positions which can be identified as disordered solvent (CH_3CN). α-$[W_{18}O_{54}(SO_3)_2]^{5-}$ incorporates two pyramidal sulfite SO_3^{2-} anions as the central cluster templates and displays an overall approximately D_{3h} symmetry, with the horizontal plane dividing the cage into two equal parts linked together by six equatorial oxo ligands (Figure 1). Unlike conventional Dawson clusters, α-$[W_{18}O_{54}(SO_3)_2]^{5-}$ shows the distinctive peanutlike shape of the $\{W_{18}O_{54}\}$ framework. Similar structures have also been observed for $\{W_{18}O_{54}\}$-type cages in the nonconventional Dawson-type compounds $(Me_4N)_6[W_{18}O_{54}(OH)_3(BiO_3)]$[22] and $(H_4N)_7[W_{18}O_{54}(O)(OH)_2(AsO_3)]$.[27] α-$[W_{18}O_{54}(SO_3)_2]^{5-}$ is almost isostructural to α-$[W_{18}O_{54}(SO_3)_2]^{4-}$ previously reported in $(Bu_4N)_4[W_{18}O_{54}(SO_3)_2]$,[30] except that they have different charges. The coordination mode for the template XO_3 is significantly different from that of XO_4 in conventional Dawson forms as described previously.[30] The orientation mode in α-$[W_{18}O_{54}(SO_3)_2]^{5-}$ allows two sulfur atoms to face each other, at a distance of 3.27 Å, with strong S−S interaction.

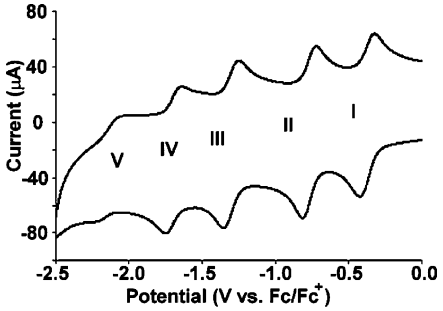

Figure 2. Cyclic voltammogram of α-$[W_{18}O_{54}(SO_3)_2]^{4-}$ in CH_3CN (0.1 M Hx_4NClO_4) at a GC electrode showing processes I to V (1×10^{-3} M; $d = 3$ mm; $\nu = 100$ mV s^{-1}).

$(Pr_4N)_4\{\alpha\text{-}[W_{18}O_{54}(SO_3)_2]\}\cdot 2CH_3CN$ crystallizes in monoclinic system with one α-$[W_{18}O_{54}(SO_3)_2]^{4-}$ anion and four Pr_4N^+ cations found in the asymmetric unit plus a number of positions for disordered solvent which sum to two CH_3CN molecules. The cluster has D_{3h} symmetry and has the same geometry as found in the compound $(Bu_4N)_4[W_{18}O_{54}(SO_3)_2]$.[30]

Electrochemical Studies. Cyclic Voltammetry of α-$[W_{18}O_{54}(SO_3)_2]^{4-}$ in CH_3CN (0.1 M Hx_4NClO_4). Preliminary investigations showed that species α-$[W_{18}O_{54}(SO_3)_2]^{4-}$ and α-$[W_{18}O_{54}(SO_3)_2]^{5-}$ are insoluble in the commonly used CH_3CN (0.1 M Bu_4NPF_6) system at the millimolar concentration level. This is also the case with the molybdosufite polyoxometalates.[29] Therefore, 0.1 M Hx_4NClO_4 was employed as the electrolyte in CH_3CN, allowing the polyoxometalates to be easily studied at the 1 mM concentration level. Figure 2 displays cyclic voltammograms obtained for reduction of α-$[W_{18}O_{54}(SO_3)_2]^{4-}$ in CH_3CN (0.1 M Hx_4NClO_4). Results are summarized in Table 2. The first two processes, labeled I and II, are well-defined one-electron steps, which are followed by further processes (III−V), which exhibit slightly more complex behavior. Processes I and II were studied over the concentration range 0.1−2 mM and the scan rate range 10−2000 mV s^{-1}. The peak height was proportional to both the concentration and the square root of scan rate under these conditions, confirming ideal diffusion-controlled behavior. The values for peak-to-peak separations ($\Delta E_p = E_p^{red} - E_p^{ox}$) obtained for processes I and II were 63 and 64 mV at a scan rate of 100 mV s^{-1}, respectively, which is very close to the predicted value of 56 mV at 20 °C for a reversible one-electron process.[39] Departure from the ideal value is attributed to some small level of uncompensated resistance. The more negative redox processes (III−V) are also chemically reversible at higher scan rates and concentrations but are affected by lower scan

(39) Bard, A. J.; Faulkner, L. R. *Electrochemical Methods*, 2nd ed.; Wiley and Sons: New York, 2001.

Table 2. Electrochemical Data Obtained by Cyclic Voltammetry for 1 mM α-$[W_{18}O_{54}(SO_3)_2]^{5-}$ and 1 mM α-$[W_{18}O_{54}(SO_3)_2]^{4-}$ at a GC Electrode (d = 3 mm) in CH_3CN (0.1 M Hx_4NClO_4); υ = 100 mV s^{-1}

species	redox process	E_f^o (V vs Fc/Fc^+)	ΔE_p (mV)
$[W_{18}O_{54}(SO_3)_2]^{5-}$	$[W_{18}O_{54}(SO_3)_2]^{5-/4-}$ (ox)	−0.357	59
	$[W_{18}O_{54}(SO_3)_2]^{5-/6-}$	−0.762	59
	$[W_{18}O_{54}(SO_3)_2]^{6-/7-}$	−1.303	74
	$[W_{18}O_{54}(SO_3)_2]^{7-/8-}$	−1.691	68
	$[W_{18}O_{54}(SO_3)_2]^{8-/9-}$	−2.143	129
$[W_{18}O_{54}(SO_3)_2]^{4-}$	$[W_{18}O_{54}(SO_3)_2]^{4-/5-}$	−0.357	63
	$[W_{18}O_{54}(SO_3)_2]^{5-/6-}$	−0.760	64
	$[W_{18}O_{54}(SO_3)_2]^{6-/7-}$	−1.295	79
	$[W_{18}O_{54}(SO_3)_2]^{7-/8-}$	−1.693	67
	$[W_{18}O_{54}(SO_3)_2]^{8-/9-}$	−2.131	86

rates and presence of trace levels of acid or protons (see later discussion). Chemical reversibility is indicated at high scan rates for all processes by the fact $I_p^{ox}/I_p^{red} \approx 1.0$. Reversible formal potentials, $E°_f$, for the five reduction processes, calculated as the average of the oxidation and reduction peak potentials [$E^o_f = (E_P^{ox} + E_P^{red})/2$], are −0.357, −0.760, −1.295, −1.693, and −2.131 V (vs Fc/Fc^+). These E^o_f values may be compared to values of −0.240, −0.615, −1.180, −1.565, −2.020, and −2.320 V (vs Fc/Fc^+) for the six one-electron processes of the sulfate salt, $(Bu_4N)_4[W_{18}O_{54}(SO_4)_2]$, reported by Zhang et al.[16] Therefore, it may be concluded that the sulfite analogue is harder to reduce than the sulfate, by ∼120−130 mV for each process. This may be attributed to the extra electron density within the cluster shell coming from the lone pairs formally associated with each SO_3 group, compared to the sulfate analogue, and this effect is felt by the metal framework thereby shifting the potentials more negative since the W centers in the sulfite case are not so electron deficient as in the sulfate case. In summary, α-$[W_{18}O_{54}(SO_3)_2]^{4-}$ is concluded to exhibit five monoelectronic reduction processes (I−V) associated with the tungsten−oxo cage of the polyoxometalate, as described by the reaction scheme in eq 1.

$$\alpha\text{-}[W_{18}O_{54}(SO_3)_2]^{4-} + e^- \rightleftharpoons \alpha\text{-}[W_{18}O_{54}(SO_3)_2]^{5-} + e^- \rightleftharpoons \alpha\text{-}[W_{18}O_{54}(SO_3)_2]^{6-} + e^- \rightleftharpoons \alpha\text{-}[W_{18}O_{54}(SO_3)_2]^{7-} + e^- \rightleftharpoons \alpha\text{-}[W_{18}O_{54}(SO_3)_2]^{8-} + e^- \rightleftharpoons \alpha\text{-}[W_{18}O_{54}(SO_3)_2]^{9-} \quad (1)$$

For a stationary electrode, when the peak current is plotted against square root of scan rate, a linear relationship is obtained. The diffusion coefficient, D, may be calculated from the Randles−Sevcik equation[39] for each of the polyoxometalate species studied to give the values reported in Table 2.

Dawson polyoxometalates usually can reversibly accept at least six electrons in aprotic solvents, probably without any structural modification in the case of the α-isomers.[1] Previous studies of the α-molybdosulfite species in CH_3CN (0.1 M Hx_4NClO_4) displayed six redox processes with reversible potentials of −0.005, −0.265, −0.885, −1.195, −1.695, and −2.075 V (vs Fc/Fc^+).[29] In the present case, it is believed that a sixth monoelectronic process forming the α-$[W_{18}O_{54}(SO_3)_2]^{10-}$ species lies beyond the negative potential electrochemical window of the CH_3CN (0.1 M Hx_4NClO_4) solvent (electrolyte) system. Assuming that the same

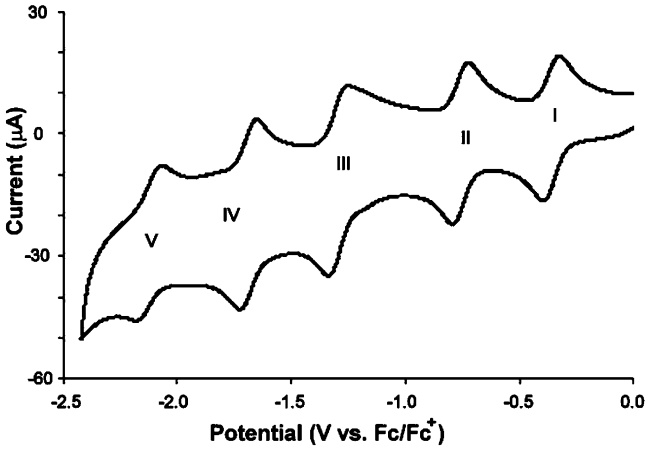

Figure 3. Cyclic voltammogram of α-$[W_{18}O_{54}(SO_3)_2]^{5-}$ in CH_3CN (0.1 M Hx_4NClO_4) at a GC electrode showing processes I−V (5×10^{-4} M; d = 3 mm; υ = 50 mV s^{-1}).

spacing exists between the redox processes for both the tungsten and molybdenum species, and also taking into account the potential differences between the sulfite and sulfate versions, leads to a prediction that the sixth monoelectronic tungsten−oxo process lies between −2.450 and −2.520 V (vs Fc/Fc^+). This very negative value is not unexpected, as generally tungsten polyoxometalates exhibit more negative reduction potentials than their molybdenum analogues.[1] This difference may be attributed to the relatively higher electron affinity of Mo(VI) sites.[16]

Given the well-separated nature of processes I and II, bulk reductive electrolysis at a fixed potential of −0.65 V can be undertaken. Coulometric analysis confirmed the expected 1.0 (±0.1) electron reduction, as the α-$[W_{18}O_{54}(SO_3)_2]^{4-}$ species is reduced to the blue α-$[W_{18}O_{54}(SO_3)_2]^{5-}$ form. As expected, in the case of α-$[W_{18}O_{54}(SO_3)_2]^{5-}$, there are also five reversible redox processes present. Again, the two initial diffusion-controlled processes, I and II, are present, but now process I is oxidative rather than reductive (ascertained from detection of faradaic current at the initial potential used in Figure 3) with an E^o_f of −0.357 V (vs Fc/Fc^+), while process II, with an E^o_f value of −0.762 V (vs Fc/Fc^+), remains a reductive process, as described by eqs 2 and 3, respectively. Processes III−V at more negative potentials also remain reductive. ΔE_p values of 59 mV are obtained for processes I and II at a scan rate of 100 mV s^{-1}, which is very close to that expected for a fully reversible diffusion controlled one-electron charge-transfer process. Voltammetric data are summarized in Table 2.

$$\alpha\text{-}[W_{18}O_{54}(SO_3)_2]^{5-} \rightleftharpoons \alpha\text{-}[W_{18}O_{54}(SO_3)_2]^{4-} + e^- \quad (2)$$

$$\alpha\text{-}[W_{18}O_{54}(SO_3)_2]^{5-} + e^- \rightleftharpoons \alpha\text{-}[W_{18}O_{54}(SO_3)_2]^{6-} \quad (3)$$

It is likely that α-$[W_{18}O_{54}(SO_3)_2]^{6-}$ and more extensively reduced species will be highly basic and react with trace amounts of water and/or dioxygen, resulting in the occurrence of processes of the kind outlined in eqs 4 and 5. Additionally, α-$[W_{18}O_{54}(SO_3)_2]^{5-}$ or more extensively reduced species may react with adventitious water (e.g., eq 6). Protonation probably explains why process III, in Figure 3, has a

shoulder, and a new process appears in the potential region between processes II and III with a decrease in concentration of α-$[W_{18}O_{54}(SO_3)_2]^{5-}$ or α-$[W_{18}O_{54}(SO_3)_2]^{6-}$. The use of lower scan rates and concentrations also adversely affect processes III−V. Previous studies have shown that the voltammetry of other highly reduced polyoxometalates also is altered significantly by the presence of adventitious proton sources.[38] This was confirmed experimentally in the present case, by noting that in the case of electrochemically synthesized α-$[W_{18}O_{54}(SO_3)_2]^{5-}$, deliberate addition of low concentrations of anhydrous triflic acid led to shifts in reversible potential values and also to the appearance of additional processes. α-$[W_{18}O_{54}(SO_3)_2]^{5-}$ solid is obtained by chemical synthesis from acidic media and voltammetric studies on the dissolved solid also provided evidence for the presence of low concentration of protonated species. In contrast, α-$[W_{18}O_{54}(SO_3)_2]^{5-}$ made by electrochemical reduction of α-$[W_{18}O_{54}(SO_3)_2]^{4-}$ did not significantly suffer from this complication.

$$2\alpha\text{-}[W_{18}O_{54}(SO_3)_2]^{6-} + O_2 + 2H_2O \rightarrow 2\alpha\text{-}[W_{18}O_{54}(SO_3)_2]^{4-} + 4OH^- \quad (4)$$

$$\alpha\text{-}[W_{18}O_{54}(SO_3)_2]^{6-} + H_2O \rightarrow \alpha\text{-}[HW_{18}O_{54}(SO_3)_2]^{5-} + OH^- \quad (5)$$

$$2\alpha\text{-}[W_{18}O_{54}(SO_3)_2]^{5-} + 2H_2O \rightarrow \alpha\text{-}[W_{18}O_{54}(SO_3)_2]^{4-} + \alpha\text{-}[H_2W_{18}O_{54}(SO_3)_2]^{4-} + 2OH^- \quad (6)$$

It is also plausible that sulfate species might be formed from oxidation of the sulfite species by reaction with molecular oxygen (eq 7). However, no evidence for the occurrence of such a reaction could be detected on the voltammetric or bulk electrolysis timescales. Addition of hydrogen peroxide to CH_3CN solution, also was not found to facilitate the oxidation of sulfite to sulfate.

$$[W_{18}O_{54}(SO_3)_2]^{m-} + O_2 \rightleftharpoons [W_{18}O_{54}(SO_4)_2]^{m-} \quad (7)$$

Hydrodynamic Voltammetry. Figure 4a displays the RDE steady-state voltammograms obtained for the α-$[W_{18}O_{54}(SO_3)_2]^{4-/5-}$ and α-$[W_{18}O_{54}(SO_3)_2]^{5-/6-}$ processes (I and II) when α-$[W_{18}O_{54}(SO_3)_2]^{4-}$ is present in bulk solution. As expected, the limiting current values, i_L, are of comparable magnitude, confirming the fact that each process involves the same number of electrons. Furthermore, the half-wave potentials or $E_{1/2}$ values calculated from the potentials when the current i has the value of $I_L/2$ are the same as E_f^o values determined from cyclic voltammetry. A plot of potential E versus $\log(i_L - i/i)$ gave a slope of 60 mV for each process, as expected for a one-electron charge-transfer reaction.

RDE voltammograms when α-$[W_{18}O_{54}(SO_3)_2]^{5-}$ is present in bulk solution (Figure 4b) are similar to those for α-$[W_{18}O_{54}(SO_3)_2]^{4-}$. That is, the $E_{1/2}$ values, wave shapes, and current magnitudes are the same as found with α-$[W_{18}O_{54}(SO_3)_2]^{4-}$, but the point of zero current now lies exactly between redox processes I and II, as expected when these initial two processes now correspond to eqs 2 and 3. Thus, the α-$[W_{18}O_{54}(SO_3)_2]^{5-/4-}$ (process I) is now oxidative in nature and gives rise to a positive current, while the α-$[W_{18}O_{54}(SO_3)_2]^{5-/6-}$ (process II) exhibits the expected negative current with a limiting current value expected for a one-electron reduction step. This result confirms that α-$[W_{18}O_{54}(SO_3)_2]^{5-}$ has indeed been isolated by one-electron bulk reductive electrolysis of α-$[W_{18}O_{54}(SO_3)_2]^{4-}$. Application of the Levich equation[39] allows the dependence of i_L on rotation rate to be investigated. Diffusion coefficient values calculated from this relationship are reported in Table 3 and within experimental error are the same as those deduced by analysis of cyclic voltammograms.

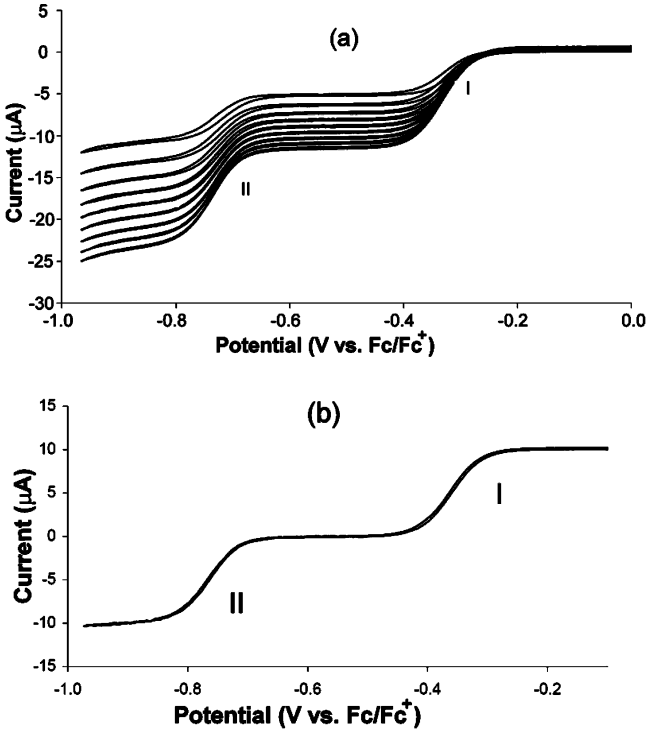

Figure 4. Rotating disc electrode voltammograms of (a) α-$[W_{18}O_{54}(SO_3)_2]^{4-}$ (bottom to top curves, $\omega = 100-1000$ rpm), and (b) electrochemically prepared α-$[W_{18}O_{54}(SO_3)_2]^{5-}$ ($\omega = 500$ rpm), in CH_3CN (0.1 M Hx_4NClO_4) at a GC electrode showing processes I and II (1×10^{-3} M; $d = 3$ mm; $v = 10$ mV s^{-1}).

Table 3. Electrochemical Data Obtained by Rotating Disc Electrode Voltammetry ($\omega = 100-500$ rpm, $v = 10$ mV s^{-1}) for 1 mM α-$[W_{18}O_{54}(SO_3)_2]^{5-}$ and 1 mM α-$[W_{18}O_{54}(SO_3)_2]^{4-}$ at a GC Electrode ($d = 3$ mm) in CH_3CN (0.1 M Hx_4NClO_4)

process		$[W_{18}O_{54}(SO_3)_2]^{5-}$	$[W_{18}O_{54}(SO_3)_2]^{4-}$
$[W_{18}O_{54}(SO_3)_2]^{4-/5-}$	$E_{1/2}$ (V)[b]	−0.354	−0.359
$[W_{18}O_{54}(SO_3)_2]^{5-/6-}$	$E_{1/2}$ (V)[b]	−0.760	−0.753
D^a ($\times 10^{-6}$ cm^2 s^{-1})		3.8	3.7

[a] D values obtained from RDE (Levich equation) and cyclic voltammetry ($v = 200-2000$ mV s^{-1}) (Randles−Sevcik equation) are identical within experimental error (±5%). [b] V vs Fc/Fc^+.

Photoactivity. Many polyoxometalates are photoactive in the presence of an appropriate electron donor. For example, the sulfate polyoxometalates $[M_{18}O_{54}(SO_4)_2]^{4-}$ (M = Mo, W) have been shown to be powerful oxidants in the presence of white light. Thus, benzyl alcohol is photo-oxidized to benzaldehyde and $[M_{18}O_{54}(SO_4)_2]^{4-}$ is multiply reduced (eq 8) when CH_3CN solutions are irradiated with white light,

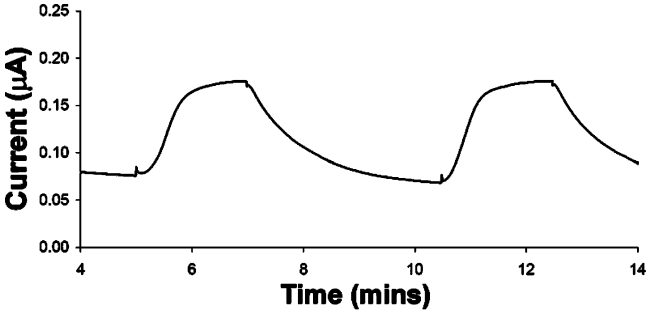

Figure 5. Current−time curves showing the photocurrents produced when $(Pr_4N)_4\{\alpha\text{-}[W_{18}O_{54}(SO_3)_2]\}\cdot 2CH_3CN$ (1×10^{-4} M) dissolved in DMF (0.1 M Bu_4NPF_6) is irradiated by white light, at a glassy carbon electrode (d = 3 mm) when the potential is held at +400 mV vs Fc/Fc^+.

and the photoelectrochemistry of $[Hx_4N]_4[M_{18}O_{54}(SO_4)_2]$ and $[Bu_4N]_4[M_{18}O_{54}(SO_4)_2]$ when DMF is used both as the solvent and as an electron donor (ED) has been postulated to occur as in eqs 9 and 10.[40−42]

$$C_6H_5CH_2OH + [M_{18}O_{54}(SO_4)_2]^{4-} \xrightarrow{h\nu} C_6H_5CHO + [H_2M_{18}O_{54}(SO_4)_2]^{4-} \quad (8)$$

$$[M_{18}O_{54}(SO_4)_2]^{4-} \xrightarrow{h\nu} \{[M_{18}O_{54}(SO_4)_2]^{4-}\}^* + ED \xrightarrow{k1} [M_{18}O_{54}(SO_4)_2]^{5-} + ED^+ \rightarrow \text{Product(s)} \quad (9)$$

$$[M_{18}O_{54}(SO_4)_2]^{5-} \xrightarrow{h\nu} \{[M_{18}O_{54}(SO_4)_2]^{5-}\}^* + ED \xrightarrow{k2} [M_{18}O_{54}(SO_4)_2]^{6-} + ED^+ \rightarrow \text{Product(s)} \quad (10)$$

In the case of the sulfite tungsten polyoxometalate, DMF solutions of $\alpha\text{-}[W_{18}O_{54}(SO_3)_2]^{4-}$ have been irradiated with white light. The large photocurrents detected imply that this polyoxometalate also is highly photoactive (Figure 5). $[W_{18}O_{54}(SO_3)_2]^{5-}$ dissolved in DMF also was found to be photoactive in the presence of white light. The reaction mechanism is assumed to be analogous to that postulated for $[M_{18}O_{54}(SO_4)_2]^{4-}$ in eqs 9 and 10.[42] Visually it was noted that a change from colorless solutions to green to blue occurs upon irradiation in the photoelectrochemical cell, as expected for formation of reduced polyoxometalates. This reaction is likely to be reversible as reversion back to the $\alpha\text{-}[W_{18}O_{54}(SO_3)_2]^{4-}$ species, presumably via oxidation by H^+ and/or O_2, is suspected by noting that the blue-colored solution reverts to green a few minutes after the light source is turned off.[40−42] Though not the main focus of this work, it is important to note the high level of photocatalytic activity of $\alpha\text{-}[W_{18}O_{54}(SO_3)_2]^{4-}$, and this will be the subject of further studies.

EPR Spectroscopy. Similar EPR spectral behavior was observed over the temperature range from 295 to 2.3 K for polycrystalline powders and ~1 mM CH_3CN solutions of chemically and electrochemically prepared $\alpha\text{-}[W_{18}O_{54}(SO_3)_2]^{5-}$. No resonances could be clearly discerned until

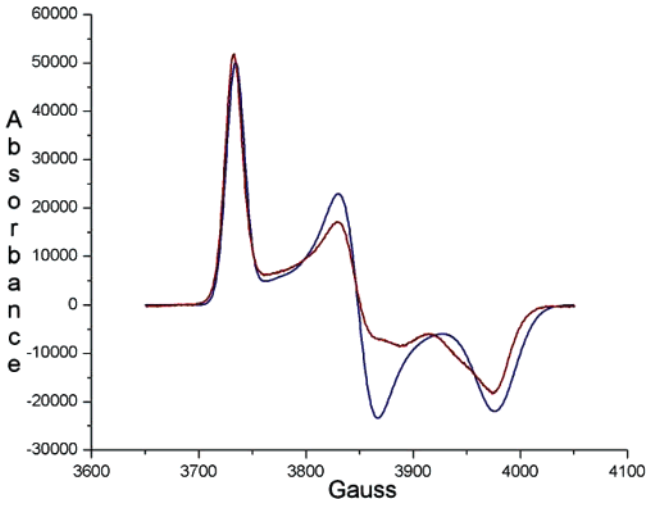

Figure 6. EPR spectra obtained from $(Pr_4N)_5\{\alpha\text{-}[W_{18}O_{54}(SO_3)_2]\}\cdot 2CH_3CN$ in CH_3CN at 2.3 K. (red line) Experimental spectrum microwave frequency 9.672 GHz, microwave power 210 nW; 100 kHz modulation amplitude 0.5 G, spectrometer gain 5.0×10^4, time constant 20.5 ms, scan rate 400G in 83.9 s. The low-intensity features at ~3890 and 3945 G are due to the "second species" referred to in the text. Simulated spectrum using the g, A, and linewidth values given in Table 4, a Gaussian line shape and with $n = 6$ is shown by the blue line.

the temperature was reduced to ~180 K, where an apparently isotropic resonance was observed with peak-to-peak derivative width of around 500 G. The resonance progressively narrowed as the temperature was reduced, being ~300 G wide at 150 K and ~200 G wide at 120 K, with $g \approx 1.79$. Below this temperature, the hitherto isotropic resonance developed a shoulder on its low-field side. At 77 K the spectra had the appearance of an axially symmetric system, with g values $g_{\|} = 1.85$ and $g_{\perp} = 1.77$. As the temperature was reduced further, the parallel peak of this axial spectrum narrowed and below about 50 K, the perpendicular peak resolved into two components. The spectrum of a ~1 mM CH_3CN solution of chemically prepared $\alpha\text{-}[W_{18}O_{54}(SO_3)_2]^{5-}$ at 2.3 K (the lowest temperature reached) and a microwave power of 200 nW (the lowest achievable) is shown in Figure 6. The main features correspond to an orthorhombic system with g values of $g_x = 1.737$, $g_y = 1.795$, and $g_z = 1.850$ and are similar to those observed for W(V) ions in sites of orthorhombic symmetry.[43,44] As a first approximation, we identify the z direction as that of the oxygen heteroanions, approximately perpendicular to the surface of the cluster, and the x and y directions as being associated with the approximate plane of the "shell" oxygens. The less-intense features observed at ~3890 and 3940 G are attributed to another species, with g values estimated as 1.783 and 1.755, respectively, and the peak due to the third g value at the same field as that of the main species, namely at ~ 3730 G ($g = 1.850$). This second species is possibly the β-isomer of $[W_{18}O_{54}(SO_3)_2]^{5-}$,[29] which symmetry-wise, is related to the γ*-form reported for the sulfate analogue.[1,29,31]

Differences between chemically and electrochemically prepared CH_3CN solutions of $\alpha\text{-}[W_{18}O_{54}(SO_3)_2]^{5-}$ were

(40) Ruther, T.; Jackson, W. R.; Bond, A. M. *Aust. J. Chem.* **2002**, *55*, 691.
(41) Ruther, T.; Jackson, W. R.; Bond, A. M. *Green Chem.* **2003**, *5*, 364.
(42) Ruther, T.; Hultgren, V. M.; Timko, B. P.; Bond, A. M.; Jackson, W. R.; Wedd, A. G. *J. Am. Chem. Soc.* **2003**, *125*, 10133.
(43) Wilson, G. L.; Greenwood, R. J.; Pilbrow, J. R.; Spence, J. T.; Wedd, A. G. *J. Am. Chem. Soc.* **1991**, *113*, 6803.
(44) Kon, H.; Sharpless, N. E. *J. Phys. Chem.* **1966**, *70*, 105.

shown by the microwave power dependence of the spectra. Chemically prepared solutions exhibited microwave power saturation effects above 1 μW at 2.3 K. The EPR spectra of α-$[W_{18}O_{54}(SO_3)_2]^{5-}$ prepared by bulk electrolysis in CH_3CN ($\sim$1 mM) showed clear evidence for longer spin relaxation times, exhibiting power saturation and adiabatic fast passage effects below about 5 K even at 200 nW microwave power levels.[45] In both cases the regions of the spectra corresponding to g_x and g_y exhibited saturation effects at lower power levels than that required for g_z The difference in the microwave power dependence of the two preparations is attributed to the presence of electrolyte in the solutions of α-$[W_{18}O_{54}(SO_3)_2]^{5-}$ prepared by bulk electrolysis. The effect of the electrolyte is to minimize solute aggregation on freezing and therefore the contribution of intermolecular interactions to the relaxation pathways.

In contrast to the analogous Mo_{18} complex where features attributable to ^{95,97}Mo hyperfine structure could be observed, no resonances attributable to ^{183}W ($I = 1/2$, 14.8% abundant) could be observed at any temperature. Complexes with a similarly coordinated W(V) ion exhibit ^{183}W hyperfine interactions of around 100×10^{-4} cm^{-1}.[43,44] For example, ^{183}W hyperfine structure is clearly observed for $[W_6O_{19}]^{3-}$, where $A_z = 126$, $A_y = A_x = 61$, and $A_o = 83 \times 10^{-4}$ cm^{-1}, respectively.[46] The corresponding values in Gauss are 158, 74, and 102, respectively. Similar magnitude hyperfine interactions have been found for other W complexes. It is therefore clear that the unpaired electron is delocalized over a number of W sites, with the hyperfine interaction being reduced in proportion to the number of these sites.

The approach to the simulation of EPR spectra for complexes where the unpaired electron is delocalized over a number of metal ion sites was described previously for the analogous Mo complexes.[29] The overall spectrum from a cluster where the unpaired electron is delocalized over n W sites is the sum of $n + 1$ spectra where the number of ^{183}W sites in each cluster, p, varies from zero to n. The relative intensity of each of these spectra can be calculated from the relative magnitudes of the terms in the binomial series expansion of $(x + y)^n = x^n(1 + y/x)^n$, where x is the fractional abundance of the $I = 0$ nuclei (0.852) and y the fractional abundance of ^{183}W (0.148). Furthermore, the width of the hyperfine structure of each component spectrum is increased in proportion to the number of ^{183}W sites in the cluster according to pA/n where A is the hyperfine interaction when the unpaired electron is localized on a single ^{183}W ion site. These considerations can be used to show that the most prominent features of the overall spectrum will be those due to clusters where all W ions have nuclei with $I = 0$ (i.e., $p = 0$) and the next most prominent would be due to clusters where only one W site is occupied by ^{183}W (i.e., $p = 1$). The experimental spectrum of Figure 6 (shown by the red line) could best be fitted with the spin Hamiltonian parameters given in Table 4 and by assuming that the unpaired electron was delocalized over three or more W sites. Simulations using the above g and A values and n between 4 and 6 are indistinguishable from those with $n = 3$ (Figure 6, blue line). A further feature of the spectrum was that the g_z peak was best simulated by a Gaussian line shape and the g_x and g_y peaks by a Lorentzian line shape. This again indicates a different relaxation mechanism for the g_z direction than for the g_x and g_y directions. The mismatch between experimental and simulated spectra in the g_y region is probably due to the differences in line shape mentioned above, the presence of the second species and to the assumption made in the simulation that the axes of g and A are coincident.

Table 4. EPR Spectral Parameters Used for the Simulation Shown in Figure 6, blue line[a]

	x	y	z
g (0.002)	1.737	1.795	1.850
A (2)	15	15	12
σ (3)	15	12	7

[a] The hyperfine interaction componenents (A) and linewidths (σ) are in units of 10^{-4} cm^{-1}. Uncertainties given in parentheses.

From the hyperfine interaction parameters in Table 4, we obtain an isotropic hyperfine interaction of $A_o = 14 \times 10^{-4}$ cm^{-1} as an upper estimate. A comparison with the value of $A_0 = 83 \times 10^{-4}$ cm^{-1} for $[W_6O_{19}]^{3-}$ where the unpaired electron is localized on a single W site, supports the view that the unpaired electron is delocalized over more than three W sites. The absence of any specific features due to W hyperfine structure makes it impossible to give a more definitive estimate, although the possibility that delocalisation occurs over six W sites is not inconsistent with the above. An analogy with the polyoxomolybdate cluster,[29] α-$[Mo_{18}O_{54}(SO_3)_2]^{5-}$ where the unpaired electron is localized over both cap regions, i.e., over a total of six metal sites, and undergoes quantum mechanical tunneling between them provides a consistent model for the orthorhombic g values, approximately isotropic A-values and the temperature dependence of the spectra as follows.

The temperature dependence of the spectrum is influenced by the rate of fluctuation of the electron density over the relevant W sites. This depends on the rate at which the local structure of the W sites distorts, the rate at which the unpaired electron hops between W sites, and the rate of quantum mechanical tunneling between sites. The first two processes are temperature dependent, whereas the third is not. If any of these rates is greater than the difference between the energies of the relevant components of the g matrix or A

(45) Abragam, A.; Bleaney, B. *Electron Paramagnetic Resonance of Transition Ions*; Clarendon Press, Oxford, 1970; Chapter 2. In order to obtain a spectrum of α-$[W_{18}O_{54}(SO_3)_2]^{5-}$ prepared by bulk electrolysis in CH_3CN free of power saturation and rapid passage effects at 2.5 K and 209 nW, a modulation frequency of 1.562 kHz and modulation amplitude of 1 G were required. The modulation frequency and amplitude dependence of the spectrum are consistent with that expected for interacting spin packets under adiabatic fast passage conditions. The role of electrolyte was shown by the observation that addition of electrolyte to a CH_3CN solution of chemically prepared α-$[W_{18}O_{54}(SO_3)_2]^{5-}$ resulted in a spectrum exhibiting power saturation and rapid passage effects similar to that of the electrochemically prepared α-$[W_{18}O_{54}(SO_3)_2]^{5-}$.

(46) Sanchez, C.; Livage, J.; Launay, J. P.; Fournier, M. *J. Am. Chem. Soc.* **1983**, *105*, 6817. The corresponding values in Gauss, as quoted in ref 47, are 158 and 74, respectively. A values in units of 10^{-4} cm^{-1} and Gauss [G] are connected by the formula $A_i(10^{-4}\ \text{cm}^{-1}) = 0.46688 \times 10^{-4}\ g_i A_i\ [G]$ (where $i = x, y, z$, or 0). See Pilbrow, J.R. *Transition Ion Electron Paramagnetic Resonance*; Clarendon Press, Oxford, 1990; Appendix A.

tensor (expressed as a frequency) an average value will be observed. Conversely, if the rates are slower, anisotropic effects will be observed. The anisotropy between the components of the *g* matrix is ~100 MHz, whereas that between the components of the hyperfine tensor, *A*, is only ~10 MHz.

As in the case of the polyoxomolybdate, the three *g* factors are explained by the unpaired electron density being delocalized predominantly over three W sites on the cap with the individual *g* and *A* principal directions oriented essentially along and perpendicular to the molecular symmetry axis. As the temperature is lowered, the molecular distortion rate slows sufficiently for the unpaired electron density to be seen as centered slightly away from the molecular symmetry axis, allowing the components of the *g* matrix to be distinguished. There are three of these off-center sites which, assuming the *z* axis is along the expected molecular axis, are rotated by 120° with respect to each other. The fluctuations in electron density involving the *z* direction and due to structural distortions and electron hopping between the W sites slow before those in the *x* and *y* directions, so that g_z is resolved below about 100 K and g_x and g_y are only below about 50 K. Quantum mechanical tunneling between the two caps introduces an additional fluctuation in the *z* direction which becomes dominant once the hopping between the W sites and the structural distortion rates are slowed sufficiently. This helps explain the apparently longer relaxation times and hence greater propensity for microwave power saturation at very low temperatures of the resonances in the *x* and *y* directions when compared with that in the *z* direction.

A feature of the present clusters is that the W−O−W bond angles linking the two halves of the molecule in the belt region are around 142° rather than the ~180° found in the conventional "Dawson" clusters.[1] The smaller bond angle will hinder transmission of electron density across the belt region and tends to confine the electron density to the surface of one-half of the cluster. However, the alignment of the sulfite oxygen atoms of the two groups relative to each other in the α-isomer could allow electron transfer via quantum mechanical tunneling between the cap regions and this would facilitate the transmission of electron density.

Conclusions

A detailed account of the synthesis, isolation, and structural characterization of the novel sulfite-based polyoxotungstate redox related pair of compounds, $(Pr_4N)_4\{\alpha\text{-}[W_{18}O_{54}(SO_3)_2]\}\cdot 2CH_3CN$ and $(Pr_4N)_5\{\alpha\text{-}[W_{18}O_{54}(SO_3)_2]\}\cdot 2CH_3CN$, has been obtained. $\alpha\text{-}[W_{18}O_{54}(SO_3)_2]^{5-}$ has a similar structure to that reported for $(Bu_4N)_4\{\alpha\text{-}[W_{18}O_{54}(SO_3)_2]\}$. $\alpha\text{-}[W_{18}O_{54}(SO_3)_2]^{5-}$ crystallizes as a monoclinic system and incorporates two pyramidal sulfite SO_3^{2-} anions as the central cluster template, with the horizontal plane dividing the cage into two equal parts linked together by six equatorial oxo ligands.

The $\alpha\text{-}[W_{18}O_{54}(SO_3)_2]^{4-/5-/6-/7-/8-/9-}$ series of reversible one-electron redox processes associated with the tungsten−oxo framework of the polyoxometalate cluster have been detailed by cyclic voltammetry. The sulfite polyoxometalate is more readily reduced than the sulfate analogue, by ~130 mV per process. Diffusion coefficient values of 3.8 and 3.7 $\times$ 10^{-6} cm^2 s^{-1} were found for $\alpha\text{-}[W_{18}O_{54}(SO_3)_2]^{5-}$ and $\alpha\text{-}[W_{18}O_{54}(SO_3)_2]^{4-}$, respectively. The sulfite-based polyoxometalate species were shown to be highly photoactive, in DMF generating photocurrents upon irradiation with white light, and exhibiting color changes indicating the formation of reduced forms of the polyoxometalate.

EPR spectra recorded down to 2.3 K provide evidence that at low temperatures the electron on $\alpha\text{-}[W_{18}O_{54}(SO_3)_2]^{5-}$ is delocalized over at least three and probably six W sites, i.e., both cap regions and undergoes quantum mechanical tunneling between them analogous to the proposal for $\alpha\text{-}[Mo_{18}O_{54}(SO_3)_2]^{5-}$.

Acknowledgment. The authors gratefully acknowledge financial support from the Leverhulme Trust (D.L. and L.C.), EPSRC (D.L. and L.C.), the Australian Research Council (A.M.B.), and the School of Physics at Monash University (J.F.B. and J.R.P.).

Supporting Information Available: Crystallographic data in cif format. This material is available free of charge via the Internet at http://pubs.acs.org.

IC062067E